THE JOURNAL OF PHYSICAL CHEMISTRY A
A JOURNAL OF THE AMERICAN CHEMICAL SOCIETY

pubs.acs.org/JPCA Article

From Molecules to Solids: A vdW-DF-C09 Case Study of the Mercury Dihalides

Valentino R. Cooper,*,§ Jaron T. Krogel, and Kelling J. Donald*,§

Cite This: J. Phys. Chem. A 2021, 125, 3978–3985 Read Online

ABSTRACT: The mercury dihalides show a remarkable diversity in the structural preferences in their minimum energy structure types, spanning molecular to strongly bound ionic solids. A challenge in the development of density functional methods for extended systems is to arrive at strategies that serve equally well such a broad range of bonding modes or structural preferences. The chemical bonding and the stabilities of mercury dihalides and the general utility and reliability of the van der Waals density functional with C09 exchange (vdW-DF-C09) in predicting or describing the energetics and structural preferences in these metal dihalides is examined. We show that, in contrast with the uncorrected generalized gradient approximation of the Perdew-Burke-Erzenhoff (PBE) exchange-correlation functional, qualitative and quantitative patterns in the bonding of the mercury dihalide solids are well reproduced with vdW-DF-C09 for the full series of HgX_2 systems for X = F, Cl, Br, and I. The possible existence of a low-temperature cotunnite polymorph for HgF_2 and PbF_2 is posited.

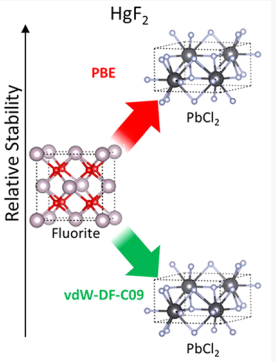

INTRODUCTION

A characteristic that is cited often as an inherent flaw in traditional density functional theory is the inability of common implementations of the exchange and correlation functionals to accurately account for dispersion interactions. This limitation arises due to the persisting need for approximate treatments of exchange and correlation in practical application. Nonetheless, various strategies exist for adding dispersion corrections to current theoretical methods, new methods formulated to include treatments for dispersion have appeared in the literature over the past several years, and additional contributions are to be anticipated as well.

A promising solution is the so-called Rutgers-Chalmers van der Waals density functional (vdW-DF).[1,2] In this approach, the dispersion interactions are accounted for in a nonlocal correlation functional. To date, this functional has been successful in describing the structure and function of a wide range of systems, including dispersion bound molecular crystals and layered materials like graphite and hexagonal boron nitride.[3−5] Recent studies have shown that, with the appropriate strategy for accounting for exchange (e.g., vdW-DF-C09[6]), these functionals are quite broadly applicable, capable of describing the physical properties of dense bulk materials such as ferroelectric ABO_3 oxides.[7,8] In this analysis, we consider the impact of van der Waals corrections on density functional methods for bulk materials with a focus on a different class of inorganic materials—the mercury dihalides—that display a wide range of structure preferences, including a number of molecular solids.

The mercury dihalides are an intriguing series of compounds in which relativistic effects and competing weak electrostatic, covalent, and ionic contributions in chemical bonding collide.[9−11] It is now well accepted that *in the gas phase*, all of the simple mercury dihalide *molecules* (HgX_2 for X = F, Cl, Br, and I) are linear.[9,12−15] It can be difficult to establish linearity unambiguously for simple triatomic molecules in matrix isolation studies, especially if the potential energy surface is flat (i.e., where the barrier to bending is very low),[12,16−20] but state-of-the-art computational investigations (and reliable electron diffraction data, where available) affirm in fact that all of the binary and ternary mercury dihalides ($HgXY$; for X = Y, and $X \neq Y$) are linear.[12,21−24]

That preference for a linear arrangement is to be expected, perhaps, since bending, which is observed in some of the group 2 dihalides, has been explained by a substantial mixing of the filled ns^2 orbital and unfilled $(n-1)$d orbital at Ca and heavier group 2 metal centers in their MX_2 molecules, if the halides are sufficiently polarizing.[20] But that kind of s−d orbital mixing is not achievable for $HgXY$ systems, because the $(n-1)d$ subshell (i.e., the set of 5d orbitals) is completely filled in Hg. That general unavailability of empty and easily accessible frontier d orbitals in Hg (and in Zn and Cd in group 12) helps to account thus for the rigidity of their linear dihalide molecules.[23,24] Indeed, a number of different research groups have shown that HgX_2 molecules are so rigid that their dimers

Received: December 4, 2020
Revised: February 6, 2021
Published: March 16, 2021

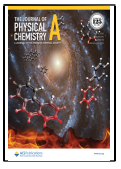

https://doi.org/10.1021/acs.jpca.0c10847
J. Phys. Chem. A 2021, 125, 3978–3985

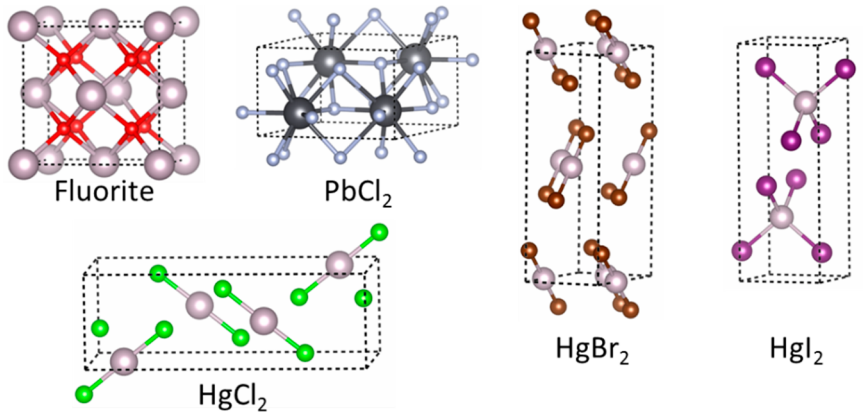

Figure 1. Stable crystal structure types of HgX_2 molecular crystals.

$(HgX_2)_2$ feature no intermonomer covalent bonding—simply HgX_2 monomers held together by weak electrostatic interactions in loose pairs.[12,21−23] And, remarkably, this characteristic of weak intermonomer interactions persists all the way through to the extended solids in some cases, but not all—with HgF_2 being the prominent exception.[25−28]

Models of structure types preferred at ambient condition when the linear HgX_2 molecules condense to form extended solids are shown in Figure 1. The preferred arrangements are the fluorite, and the namesake $HgCl_2$, $HgBr_2$, and red HgI_2 types for X = F, Cl, Br, and I, respectively.

The mercury dibromide and diiodide structures have at least one other competitive or metastable structure in each case that is not included in Figure 1.[25,26,29−31] The nature and relative stabilities of the several polymorphs of HgI_2 that can (co)exist at ambient conditions have been discussed in detailed reports by Hostettler and Schwarzenbach.[25,26] The $PbCl_2$ (cotunnite) structure type[32,33] is included in Figure 1 as a reference for discussion later on in this report.

The dependence of the HgX_2 structural preferences on X is striking. As we just mentioned, the heavier dihalides form molecular solids at ambient conditions,[29] and there is even experimental evidence that HgH_2 forms a molecular extended solid as well.[34] The most stable form of HgI_2 is a red layered structure with vertex-linked tetrahedra, but the metastable yellow form, for example, is a molecular solid.[25,26] Yet, the fluoride adopts unequivocally the ionic fluorite structure[25,35]—a fact that may be attributed to the polarity or strong ionic character of the Hg−F bonds.[23] So, even though the minimum energy dimer and trimer of HgF_2 are found computationally to be weak assemblies of linear monomers (just like all of the other Hg dihalides),[12,21−23,36,37] the accumulating crystal packing forces and the increasing polarization of the Hg centers stabilize an ionic (fluorite) solid.[11,37] For the HgX_2 solids where X is less electronegative (Cl, Br, and I), no such ionic alternative is observed in theory or experiment; they rely substantially on weak interactions.[23]

Given this diversity in the bonding in the HgX_2 solids, therefore, and the significant role of dispersion forces in some cases, we have selected this series of structures for a detailed analysis of the performance of the vdW-DF-C09 method and its ability to accurately model bonding preferences and relative stabilities.

We find that vdW-DF-C09 reproduces, with good success, key experimental results available for the mercury dihalides. Importantly, our calculations affirm recent claims that the $PbCl_2$ structure is competitive for HgF_2 at low temperatures,[38] a result that is consistent with observations for a similar compound, PbF_2, as well. It has been shown in a recent high-pressure study of HgF_2, in line with an earlier computational investigation,[39] that the $PbCl_2$ type polymorph may coexist with the fluorite structure at ambient temperatures and moderate pressures. In assessing the versatility of vdW-DF-C09 as a general-purpose density functional, we raise the question of whether low temperatures may induce this transition as well, inviting a more expansive elucidation of the phase diagram for the mercury dihalides. The relevance of the method to ionic and covalent systems and long-range interactions is demonstrated.

■ COMPUTATIONAL METHODS

All DFT calculations were performed using the van der Waals density nonlocal correlation functional with the C09 exchange functional (vdW-DF-C09)[1,2,6] and ultrasoft pseudopotentials as implemented in the Quantum Espresso simulation package.[40] The electronic configurations of the ions were Hg: $5d^{10}6s^2$, F: $2s^22p^5$, Cl: $3s^23p^5$, Br: $4s^24p^5$, and I: $5s^25p^5$. K-point meshes of 1 × 1 × 1 and 8 × 8 × 8 were employed for the HgX_2 monomers and dimers, and bulk solids, respectively. A 140 Ry planewave cutoff was used for all calculations, and the forces on the atoms were relaxed until they were less than 5 meV/Å. For bulk solids, all lattice constants were fully optimized. Comparisons with the MP2 method[41] and the generalized gradient approximation of Perdew-Burke-Erzenhoff (PBE) exchange-correlation functional,[42] which does not account for dispersion interactions, were carried out in order to understand the effects of dispersion interactions in the molecular systems studied in this work. PBE values with the D3 dispersion correction (PBE-D3)[43] are also included for optimized bulk HgX_2 for comparison. It should be noted that although the vdW-DF class of functionals was designed to treat dispersion interactions within the DFT framework, recent studies of condensed matter systems indicate that the functional is indeed a general-purpose functional, capable of successfully modeling systems with ionic and covalent bonding as well as weak attractive interactions.[3−5,7,8] High-throughput DFT calculations were monitored and conducted using the Nexus workflow management system, which is an open source code (see https://www.qmcpack.org/nexus).[44] The script is available in the Supporting Information (SI).

https://doi.org/10.1021/acs.jpca.0c10847
J. Phys. Chem. A 2021, 125, 3978−3985

RESULTS AND DISCUSSION

Figure 2 illustrates the minimum energy geometry of the HgX_2 dimer and five parameters that may be used to characterize it.

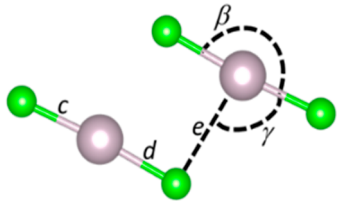

Figure 2. Structural parameters for HgX_2 dimer geometry.

The values of these parameters, which were obtained from previous MP2 calculations[23] and from our DFT vdW-DF-C09 and PBE calculations in this work are listed in Table 1.

All three methods agree on the general C_{2h} structure of the dimers, but we find significant differences in the magnitudes of the monomer−monomer interaction energies ($\Delta E_{int} = E_{dimer} - 2E_{(free\text{-}monomer)}$) and in qualitative trends. All three methods predict that the HgF_2 dimer has the strongest interaction energy, with the MP2 and vdW-DF-C09 methods exhibiting shorter contacts and larger binding energies overall. For the PBE method, the heavier dimer pairs all have similar interaction energies (−0.14 ± 0.01 eV in Table 1).

This discrepancy in PBE behavior is most likely a direct consequence of the poor description of dispersion interactions in that semilocal exchange-correlation functional. On the other hand, the MP2 and vdW-DF-C09 methods show an initial decrease in the dimer binding energy going down the halide series but recovers some binding for the HgI_2 dimer.

The trends in the MP2 and the vdW-DF-C09 data as well as the deviations of the PBE results can be easily understood considering the relative ionicity of the Hg−*X* bond and the polarizability of the atoms involved, especially as X gets larger. Previous work by Donald and co-workers demonstrated that, for the HgX_2 series, as we go up group 17 from I to F, there is an increase in the ionic contribution to Hg−*X* bonds.[23] In other words, much more charge density is transferred from Hg to F than from Hg to I. This is a direct result of a substantial increase in electronegativity as you move up the halide series from I to F, and the increases in the Hg−F charge transfer as *X* gets smaller results in increased dipole−dipole interactions between adjacent Hg−F bonds in the dimers (Figure 2). This significantly stabilizes the intermolecular interactions in the HgF_2 dimer. This type of interaction is well accounted for by traditional density functionals and may explain why the PBE functional yields dimer binding energies comparable to those obtained with vdW-DF-C09 for HgF_2.

As the size of the X atom increases going from F to I, however, there is a correspondingly substantial increase in its polarizability, leading to an increase in the dispersion contribution to the intermonomer bonding. The overall bonding in the dimers, therefore, is expected to be an interplay between London dispersion, dipole−dipole, and charge transfer interactions, with the latter decreasing as the *X* atoms get larger.

The differences in the magnitudes of the vdW-DF-C09 interactions and the MP2 values in Table 1 are in line with a tendency for the MP2 method to overbind in some cases, and there may be potential differences as well when including relativistic effects in DFT calculations. Nevertheless, we believe that in this case the vdW-DF-C09 calculations give reasonable descriptions of the binding in these systems and are suitable starting points for exploring the properties of the bulk solids for the mercury dihalides as well.

Table 2 lists the structural parameters for the ground state structures studied for each of the four HgX_2 structures. For all of the structures (where data are available), we find that the vdW-DF-C09 method significantly improves agreement with the experimentally determined structural parameters[25,28,30,31,35] relative to the PBE results. For the latter method, the lack of dispersion contributions results in a significant overestimation of lattice parameters along the dispersion bound axes of the unit cell (Table 2)—for $HgCl_2$, $HgBr_2$, and HgI_2 the lattice parameters are overshot by up to ∼10%. We note considerable improvement in PBE structural parameters when we include the Grimme-D3 correction (see Table 2), and the vdW-DF-C09 lattice parameters are all typically within 2.5% of the experimental values; with the majority of systems giving errors of less than 1%. One exception to this, however, is $HgBr_2$, where vdW-DF-C09 underestimates the *a*-axis lattice parameter by 7.6%. Furthermore, vdW-DF-C09 gives an improved agreement (over PBE) relative to experiment for HgF_2, PbF_2, and CaF_2 in the fluorite structure type, which is the global minimum at ambient conditions for all three systems. These results affirm

Table 1. Geometrical Parameters and Monomer−Monomer Interaction Energies (ΔE) for HgX_2 Dimers Obtained at the MP2, vdW-DF-C09, and PBE Levels[a]

dimer	method	*c* [Å]	*d* [Å]	*e* [Å]	*β* [deg]	*γ* [deg]	ΔE [eV]
HgF_2	MP2	1.899	1.929	2.656	177.9	108.6	−0.62
	vdW-DF-C09	1.924	1.958	2.628	177.0	108.3	−0.38
	PBE	1.938	1.971	2.700	176.9	109.1	−0.31
$HgCl_2$	MP2	2.229	2.251	3.166	176.9	96.9	−0.24
	vdW-DF	2.256	2.285	3.074	175.3	98.1	−0.30
	PBE	2.270	2.295	3.242	175.8	98.9	−0.15
$HgBr_2$	MP2	2.358	2.379	3.239	175.3	95.5	−0.22
	vdW-DF	2.402	2.434	3.153	172.8	98.0	−0.31
	PBE	2.418	2.444	3.332	174.0	97.8	−0.15
HgI_2	MP2	2.540	2.559	3.460	173.7	94.5	−0.24
	vdW-DF	2.592	2.631	3.242	167.5	100.5	−0.33
	PBE	2.610	2.638	3.463	170.6	98.7	−0.13

[a]The geometrical parameters *c*, *d*, *e*, *β*, and *γ* are defined as in Figure 2.

https://doi.org/10.1021/acs.jpca.0c10847
J. Phys. Chem. A 2021, 125, 3978−3985

Table 2. Lattice Parameters *a*, *b*, and *c* for the Preferred Molecular Crystal Structures for the HgX_2 Series[a]

system	space group	method	*a* [Å]	*b* [Å]	*c* [Å]
[b]HgF_2 (fluorite)	$Fm\bar{3}m$	PBE	5.635	–	–
		PBE-D3	5.635	–	–
		vdW-DF	5.531	–	–
		expt.	5.54(1)	–	–
HgF_2 (cotunnite)	*Pnma*	PBE	5.933	3.883	7.714
		PBE-D3	5.996	3.783	7.285
		vdW-DF	5.956	3.644	7.079
		expt.	–	–	–
[b]$HgCl_2$	*Pnma*	PBE	13.373	6.578	4.514
		PBE-D3	12.829	6.260	4.362
		vdW-DF	12.458	5.873	4.220
		expt.	12.765(6)	5.972(3)	4.330(2)
[b]$HgBr_2$	$Cmc2_1$	PBE	5.063	7.026	13.653
		PBE-D3	4.658	6.903	12.730
		vdW-DF	4.272	6.857	12.336
		expt.	4.628(2)	6.802(2)	12.476(2)
[b]*red* HgI_2	$P4_2/nmc$	PBE	4.509	–	14.025
		PBE-D3	4.475	–	13.945
		vdW-DF	4.364	–	12.205
		expt.	4.361(5)	–	12.450(7)
yellow HgI_2	$Cmc2_1$	PBE	5.317	7.552	14.416
		PBE-D3	4.624	7.663	14.188
		vdW-DF	4.437	7.368	13.362
		expt.	4.734(1)	7.408(2)	13.943(3)
[b]PbF_2 (fluorite)	$Fm\bar{3}m$	PBE	6.008	–	–
		vdW-DF	5.906	–	–
		expt.	5.931	–	–
PbF_2 (cotunnite)	*Pnma*	PBE	6.582	3.950	7.831
		vdW-DF	6.372	3.856	7.624
		expt.	6.4567(9)	3.9071(5)	7.666(1)
[b]CaF_2 (fluorite)	$Fm\bar{3}m$	PBE	5.509	–	–
		vdW-DF	5.422	–	–
		expt.	5.471	–	–
CaF_2 (cotunnite)	*Pnma*	PBE	6.005	7.076	3.642
		vdW-DF	5.899	6.951	3.544
		expt.	–	–	–

[a]Competing structures for both HgF_2 and HgI_2 are included for completeness. Additionally, the fluorite and $PbCl_2$ structures for PbF_2 and CaF_2 are included for later comparisons between the PBE and vdW-DF methods. [b]Indicates the experimentally determined ground state structure type at ambient conditions.

the general applicability of the vdW-DF-C09 functional for different types of materials and bonding modes.

To further examine the viability of the nonlocal functional for molecular crystal structure prediction, we computed and compared condensation energies for the HgX_2 systems in the four most relevant structures; fluorite (HgF_2), $HgCl_2$, $HgBr_2$, and *red*-HgI_2.

The condensation energy, $\Delta E_{condens}$, is computed as

$$\Delta E_{condens} = E_{mol} - \frac{1}{n} E_{solid} \quad (1)$$

where E_{mol} and E_{solid} are the total energies of the HgX_2 isolated molecule and solid, respectively. *n* is the number of HgX_2 units in the unit cell of the relevant extended solid. Figure 3 depicts the condensation energies for $HgCl_2$, $HgBr_2$, and HgI_2 in the four crystal structures studied. It should be noted that the condensation energies for different crystal structures of HgF_2 were also studied, but in most cases, the starting crystal structures, other than the fluorite (HgF_2) structure, were unstable and relaxed to the fluorite structure. Nevertheless, a striking observation is that the condensation energies for $HgCl_2$, $HgBr_2$, and HgI_2 obtained using vdW-DF-C09 are considerably larger than those determined with the PBE functional. This is a direct indication of the significance of dispersion interactions in defining the stability of these structures. Interestingly, we find that dispersion interactions even stabilize the densely packed fluorite structure, which is found to be largely unstable at the PBE level for all three HgX_2 structure considered in Figure 3. We note that the PBE-D3 functional exhibits similar trends for dispersion bound complexes as observed for the vdW-DF-C09. It is worth noting that similar results were previously observed for comparisons between vdW-DF-C09 and the Becke-Johnson parametrization of PBE-D3.[45] One key feature seems to be a systematic difference in the total condensation energy with the vdW-DF-C09 being almost ~0.40 eV lower that the PBE-D3 values (see Figure S1 in the Supporting Information). This could be related to the tendency for the vdW-DF-C09 functional to overbind materials. However, the PBE-D3 shows similar behavior to the PBE functional for the

https://doi.org/10.1021/acs.jpca.0c10847
J. Phys. Chem. A 2021, 125, 3978−3985

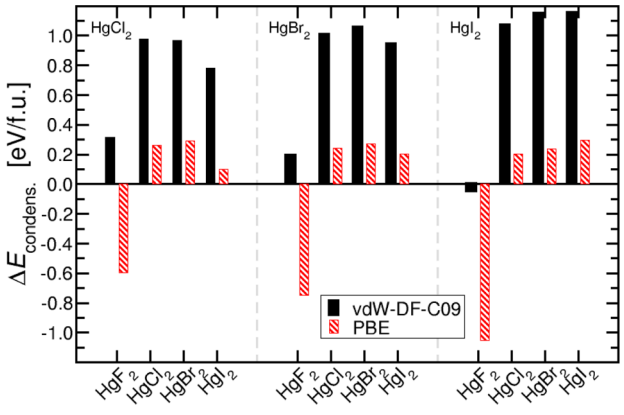

Figure 3. Condensation energy for $HgCl_2$, $HgBr_2$, and HgI_2 for the four possible crystal structures considered. vdW-DF-C09 and PBE calculations are represented by black, solid bars and red, hashed bars, respectively. In all cases, the reference energy is the isolated HgX_2 molecule. A similar plot for PBE-D3 can be found in the Supporting Information, Figure S2. The values are given in electron volts per formula unit (eV/f.u.).

condensed matter fluorite structure (see Figure S2 in the Supporting Information), resulting in nearly the same lattice constants for some halide ions. This behavior may be related to the PBE-D3 damping function, which would turn off at typical ionic bonding distances.

As shown in Table 3, we observe a similar trend in the predicted ground state condensation energies as in the isolated

Table 3. Condensation Energies for the Ground State Structures Predicted Using the PBE, PBE-D3, and vdW-DF-C09 Methods[a]

	$\Delta E_{condensation}$ [eV/f.u.]		
system	PBE	PBE-D3	vdW-DF-C09
HgF_2	0.658	1.161	1.316
$HgCl_2$	0.289 (0.260)	0.749	0.978
$HgBr_2$	0.273	0.787	1.056
HgI_2	0.296	0.903	1.156

[a]For $HgCl_2$, PBE finds the $HgBr_2$ structure type to be the ground state, so we include it here as well as the PBE values for the experimentally observed $HgCl_2$ ground state structure in parentheses.

dimers. Specifically, for PBE calculations, we find that the HgF_2 structure has the strongest condensation energy (0.658 eV), while the remaining structures all have very similar condensation energies (0.27−0.29 eV).

On the other hand, we find for vdW-DF-C09 (and PBE-D3) that the HgF_2 structure again has the largest condensation energy, but as we move down the table from $HgCl_2$ to HgI_2, there is an overall increase in the condensation energy of roughly 0.2 eV per formula unit (eV/f.u.). This latter observation can be related to two factors: (1) as you go down group 17 in the periodic table, the dispersion interactions between the HgX_2 monomers should increase, commensurate with the size of the halide ions and (2) the enhanced alignment of bond dipoles going from $HgCl_2$ to HgI_2 and the eventual condensation into a layered structure in HgI_2, which itself arises from (and is evidence for) an enhancement of monomer−monomer interactions. Interestingly, this trend remains if we consider all three halide compounds in the same structure type, where—in the $HgBr_2$ structure type—the vdW-DF-C09 condensation energies are 0.966, 1.056, and 1.147 eV/f.u. for $HgCl_2$, $HgBr_2$, and HgI_2, respectively (Figure 3). This suggests that the driving force in these materials is most likely enhancements in dispersion interactions due to increased atom size.

For $HgCl_2$, as previously discussed, we find that PBE calculations predict the $HgBr_2$ structure type to be the ground state by 29 meV/f.u. over the experimentally observed $HgCl_2$ structure type.[46] On the other hand, vdW-DF-C09 predicts the $HgCl_2$ structure to be the most stable structure (by 12 meV/f.u.). This failure of the PBE functional can be easily understood as well on the basis of the nature of the crystal structures and the lack of dispersion interaction contributions. In the $HgBr_2$ structure, unlike $HgCl_2$, the molecular units are aligned such that the Hg−X bonds are parallel and shifted to ensure that opposing dipoles interact favorably with each other. Thus, in the absence of dispersion interactions, one might expect that this structure would be preferred over one in which certain molecules are arranged perpendicularly to each other (as in $HgCl_2$). This uniquely highlights the balance between ionicity and weak dispersion or van der Waals interactions in defining the properties of these compounds.

Another feature that comes out of the vdW-DF-C09 results is the close proximity in energy (∼9 meV/f.u.) of the $HgBr_2$ structure type to that of the red HgI_2 structure for the HgI_2 molecular crystal structures (as opposed to 59 meV/f.u. in the PBE calculations). This is remarkable given that it is known that the $HgBr_2$ crystal structure[29,30] (denoted as the yellow$_M$ HgI_2 structure in refs 25 and 26) is a competing polymorph that exists under ambient conditions. These results again signal the superior performance of vdW-DF-C09 for exploratory studies of a wide range of molecular crystal structures.

A final consideration is the crystal structure of HgF_2. As previously noted, both PBE and vdW-DF-C09 overwhelmingly find the fluorite structure to be the ground state structure when compared with the above-mentioned alternative crystal structures, namely $HgCl_2$, $HgBr_2$, and HgI_2. However, a recent PBE study demonstrated that under pressure it may be possible to transform the fluorite structure into the $PbCl_2$ structure at ∼5 GPa.[38] Using the above methods, we compared the stability (condensation energies) of this structure using both PBE and vdW-DF-C09. Surprisingly, we found that although PBE retains the fluorite structure as the ground state, vdW-DF-C09 predicts the $PbCl_2$ structure to be the ground state structure by 20 meV/f.u. (see Figure 4).

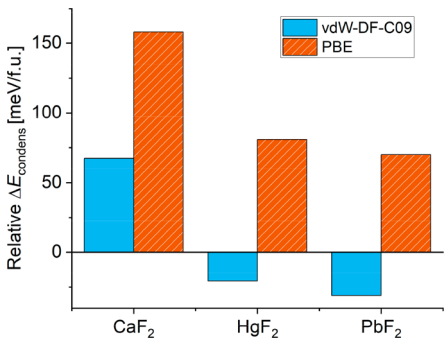

Figure 4. Relative condensation energies for the fluorite versus $PbCl_2$ structure for CaF_2, HgF_2, and PbF_2 obtained using PBE (red striped) and vdW-DF-C09 (solid blue). Positive values indicate that the fluorite structure is the most stable structure.

https://doi.org/10.1021/acs.jpca.0c10847
J. Phys. Chem. A 2021, 125, 3978−3985

To better understand this, we compared the behavior of vdW-DF-C09 and PBE for two similar materials: CaF_2 and PbF_2. As expected, the fluorite structure is predicted to be the ground state for CaF_2, the prototypical fluorite material. Conversely, for PbF_2, we observe a similar behavior as in HgF_2, where vdW-DF-C09 predicts the $PbCl_2$ structure to be more stable in contrast to the PBE calculations, which favor the fluorite structure. Unlike HgF_2, however, the phase diagram (above room temperature) has been extensively mapped out for PbF_2. Here, we find that for PbF_2, the $PbCl_2$ and fluorite structures coexist under ambient pressures and temperatures.[47] Furthermore, a small amount of pressure results in a complete (and irreversible) transformation into the $PbCl_2$ structure, while high temperatures are necessary to produce a reversible transformation into the fluorite structure.[47] This phase diagram seems to hint at the stability of the $PbCl_2$ structure for PbF_2 and that lower temperatures may stabilize this phase. In the context of our observations for PbF_2, we consider that it is likely that the true ground state for HgF_2 may indeed be $PbCl_2$ at low temperatures and, at ambient temperatures and pressures, the fluorite and $PbCl_2$ phases may coexist.

SUMMARY AND OUTLOOK

Exceptional features of the crystal structure preferences of the group 12 dihalides and the critical role of dispersion interactions in accounting for those preferences provide the arena in which we assess the utility of the nonlocal Rutgers-Chalmers van der Waals density correlation functional with the C09 exchange functional (vdW-DF-C09) compared to the more commonly employed Perdew-Burke-Erzenhoff (PBE) exchange-correlation functional. Both density functional approximations are considered with regard to their success in reproducing the structural preferences of the HgF_2 extended solid as well as the molecular crystal structures of the heavier HgX_2 compounds. The difluoride is known to adopt the ionic fluorite structure type, while all of the other systems tend to prefer or have metastable incarnations of molecular structure types; mercury dichloride and dibromide have molecular global minima, and mercury diiodide has a metastable local minimum even though a two-dimensional layered structure has been found to be the global minimum at ambient conditions.

The vdW-DF-C09 approximation shows superior performance relative to the more commonly implemented PBE functional in predicting the structural preferences of the global and low-energy local minima of the series of dihalides. In particular, the vdW-DF-C09 identifies correctly the global minimum energy structure—from among a set of four alternative starting structure types—for each of the four mercury dihalides. This dispersion corrected method recovers the correct geometrical preference for all of the dihalides, confirming that the fluorite structure adopted by HgF_2 is not competitive for any of the heavier HgX_2 systems. In contrast, the PBE approximation identifies the $HgBr_2$ structure (though by a small margin of ~0.29 meV over the experimentally observed $HgCl_2$ structure type) as the global minimum for $HgCl_2$ solid and uniformly underestimates the binding in the dimers and extended solids of all of the dihalides. That is especially clear for the three heaviest cases where polarization is critical due to the softness (high polarizabilities) of Cl, Br, and I.

The vdW-DF-C09 method gives noticeably better agreement overall with the experimental lattice parameters for the minimum energy structures and achieves a significant enhancement in the condensation energy just mentioned for all of the metal dihalides relative to the PBE method. Of note, the vdW-DF-C09 method predicts a lower energy for the $PbCl_2$ structure type for HgF_2 and PbF_2, for which the fluorite structure has long been considered to be the minimum energy geometry at ambient conditions. That, on the face of it, would appear to betray limitations to the method, but a phase diagram for PbF_2 reveals that the metastable orthorhombic α-$PbCl_2$ type polymorph can coexist with the cubic fluorite at ambient conditions and is stabilized at lower temperatures. Our results suggest that the same may be true for HgF_2, inviting new low-temperature experimental studies to complement some evidence that has recently been reported for high pressures.[38,39]

ASSOCIATED CONTENT

Supporting Information

The Supporting Information is available free of charge at https://pubs.acs.org/doi/10.1021/acs.jpca.0c10847.

Graphical comparison of computed vdW-DF-C09 and PBE-D3 condensation energies with a strong linear correlation for the mercury dihalides in different structure types, the actual condensation energies obtained for the PBE-D3 method, and the NEXUS script for computational simulation workflow management (PDF)

AUTHOR INFORMATION

Corresponding Authors

Valentino R. Cooper − *Materials Science and Technology Division, Oak Ridge National Laboratory, Oak Ridge, Tennessee 37830, United States;* orcid.org/0000-0001-6714-4410; Phone: 1-865-574-5164; Email: coopervr@ornl.gov

Kelling J. Donald − *Department of Chemistry, Gottwald Center for the Sciences, University of Richmond, Richmond, Virginia 23173, United States;* orcid.org/0000-0001-9032-4225; Phone: 1-804-484-1628; Email: kdonald@richmond.edu

Author

Jaron T. Krogel − *Materials Science and Technology Division, Oak Ridge National Laboratory, Oak Ridge, Tennessee 37830, United States;* orcid.org/0000-0002-1859-181X

Complete contact information is available at: https://pubs.acs.org/10.1021/acs.jpca.0c10847

Author Contributions

[§]V.R.C. and K.J.D. contributed equally to this work.

Notes

This manuscript has been authored by UT-Battelle, LLC under Contract No. DE-AC05-00OR22725 with the U.S. Department of Energy. The United States Government retains and the publisher, by accepting the article for publication, acknowledges that the United States Government retains a nonexclusive, paid-up, irrevocable, worldwide license to publish or reproduce the published form of this manuscript, or allow others to do so, for United States Government purposes. The Department of Energy will provide public access to these results of federally sponsored research in accordance with the DOE Public Access Plan (http://energy.gov/downloads/doe-public-access-plan).

The authors declare no competing financial interest.

■ ACKNOWLEDGMENTS

This work was supported by the U.S. Department of Energy, Office of Science, Basic Energy Sciences, Division of Materials Sciences and Engineering. K.J.D. acknowledges sabbatical support through the ORNL HERE program, sponsored by the U.S. DOE and administered by the Oak Ridge Institute for Science and Education and by the University of Richmond, and funding from the National Science Foundation (CHE-1056430). This work used resources of the National Energy Research Scientific Computing Center, which is supported by the Office of Science of the U.S. Department of Energy under Contract No. DE-AC02-05CH11231. All figures molecular structures/crystals were drawn with the VESTA program.[48]

■ REFERENCES

(1) Dion, M.; Rydberg, H.; Schröder, E.; Langreth, D. C.; Lundqvist, B. I. van der Waals density functional for general geometries. *Phys. Rev. Lett.* **2004**, *92*, 246401.
(2) Thonhauser, T.; Cooper, V. R.; Li, S.; Puzder, A.; Hyldgaard, P.; Langreth, D. C. van der Waals density functional: Self-consistent potential and the nature of the van der Waals bond. *Phys. Rev. B: Condens. Matter Mater. Phys.* **2007**, *76*, 125112.
(3) Berland, K.; Chakarova-Kack, S. D.; Cooper, V. R.; Langreth, D. C.; Schroder, E. A van der Waals density functional study of adenine on graphene: single-molecular adsorption and overlayer binding. *J. Phys.: Condens. Matter* **2011**, *23*, 135001.
(4) Berland, K.; Cooper, V. R.; Lee, K.; Schröder, E.; Thonhauser, T.; Hyldgaard, P.; Lundqvist, B. I. van der Waals forces in density functional theory: A review of the vdW-DF method. *Rep. Prog. Phys.* **2015**, *78*, No. 066501.
(5) Cooper, V. R.; Kong, L.; Langreth, D. C. Computing dispersion interactions in density functional theory. *Phys. Procedia* **2010**, *3*, 1417.
(6) Cooper, V. R. van der Waals density functional: An appropriate exchange functional. *Phys. Rev. B: Condens. Matter Mater. Phys.* **2010**, *81*, 161104.
(7) Yuk, S. F.; Pitike, K. C.; Nakhmanson, S. M.; Eisenbach, M.; Li, Y. W.; Cooper, V. R. Towards an accurate description of perovskite ferroelectrics: Exchange and correlation effects. *Sci. Rep.* **2017**, *7*, 43482.
(8) Berland, K.; Arter, C. A.; Cooper, V. R.; Lee, K.; Lundqvist, B. I.; Schroder, E.; Thonhauser, T.; Hyldgaard, P. van der Waals density functionals built upon the electron-gas tradition: Facing the challenge of competing interactions. *J. Chem. Phys.* **2014**, *140*, 18A539.
(9) Liao, M.-S.; Zhang, Q.-E.; Schwarz, W. H. E. Properties and Stabilities of *MX*, MX_2, and M_2X_2 Compounds (*M* = Zn, Cd, Hg; *X* = F, Cl, Br, I). *Inorg. Chem.* **1995**, *34*, 5597.
(10) von Szentpály, L. Hard Bends Soft: Bond Angle and Bending Force Constant Predictions for Dihalides, Dihydrides, and Dilithides of Groups 2 and 12. *J. Phys. Chem. A* **2002**, *106*, 11945.
(11) Donald, K. J.; Kretz, W. J.; Omorodion, O. The HgF_2 Ionic Switch: A Triumph of Electrostatics against Relativistic Odds. *Chem. - Eur. J.* **2015**, *21*, 16848.
(12) Kaupp, M.; von Schnering, H. G. Dominance of linear 2-coordination in mercury chemistry: Quasirelativistic and non-relativistic *ab initio* pseudopotential study of $(HgX_2)_2$ (*X* = F, Cl, Br, I, H). *Inorg. Chem.* **1994**, *33*, 2555.
(13) Greenwood, N. N.; Earnshaw, A. *Chemistry of the Elements*, 2nd ed.; Elsevier, 1997.
(14) Hargittai, M. Molecular structure of metal halides. *Chem. Rev.* **2000**, *100*, 2233.
(15) Balabanov, N. B.; Peterson, K. A. A systematic *ab initio* study of the structure and vibrational spectroscopy of $HgCl_2$, $HgBr_2$, and HgBrCl. *J. Chem. Phys.* **2003**, *119*, 12271.
(16) Givan, A.; Loewenschuss, A. The infrared and Raman spectra of matrix isolated binary and mixed mercury halides. *J. Chem. Phys.* **1976**, *64*, 1967.
(17) Givan, A.; Loewenschuss, A. A critical evaluation of spectroscopic parameters from vibrational isotopic effects in matrix isolated MX_2 and *MXY* molecules (*M* = Zn, Cd, Hg; *X*, *Y* = Cl, Br, I). *J. Mol. Struct.* **1978**, *48*, 325.
(18) Givan, A.; Loewenschuss, A. Matrix isolation infrared and Raman spectra of binary and mixed group II B fluorides. *J. Chem. Phys.* **1980**, *72*, 3809.
(19) Varga, Z.; Lanza, G.; Minichino, C.; Hargittai, M. Quasilinear molecule par excellence, $SrCl_2$: Structure from high-temperature gas-phase electron diffraction and quantum-chemical calculations–computed structures of $SrCl_2$·Argon complexes. *Chem. - Eur. J.* **2006**, *12*, 8345.
(20) Kaupp, M. Non-VSEPR" Structures and Bonding in *d*0 Systems. *Angew. Chem., Int. Ed.* **2001**, *40*, 3534.
(21) Kaupp, M.; von Schnering, H. G. *Ab Initio* Comparison of the $(MX_2)_2$ Dimers (*M* = Zn, Cd, Hg; *X* = F, Cl, H) and Study of Relativistic Effects in Crystalline HgF_2. *Inorg. Chem.* **1994**, *33*, 4718.
(22) Ruberto, R.; Pastore, G.; Özen, A. S.; Akdeniz, Z.; Tosi, M. P. Static and dynamic structure of monomers, dimers and trimers of $HgCl_2$ from density-functional calculations. *Eur. Phys. J. D* **2012**, *66*, 229.
(23) Donald, K. J.; Hargittai, M.; Hoffmann, R. Group 12 dihalides: Structural predilections from gases to solids. *Chem. - Eur. J.* **2009**, *15*, 158.
(24) Prasad, S.; Wittmaack, B. K.; Donald, K. J. Bending Ternary Dihalides. *J. Phys. Chem. A* **2018**, *122*, 9065.
(25) Hostettler, M.; Schwarzenbach, D. Phase diagrams and structures of HgX_2 (*X* = I, Br, Cl, F). *C. R. Chim.* **2005**, *8*, 147.
(26) Hostettler, M.; Birkedal, H.; Schwarzenbach, D. Polymorphs and Structures of Mercuric Iodide. *CHIMIA Int. J. Chem.* **2001**, *55*, 541.
(27) Braekken, H.; Scholten, W. The Crystal Structure of Mercuric Chloride. *Z. Kristallogr.* **1934**, *89*, 448.
(28) Subramanian, V.; Seff, K. Mercuric chloride, a redetermination. *Acta Crystallogr., Sect. B: Struct. Crystallogr. Cryst. Chem.* **1980**, *36*, 2132.
(29) Braekken, H. The Crystal Structure of Mercuric Bromide. *Z. Kristallogr.* **1932**, *81*, 152.
(30) Jeffrey, G. A.; Vlasse, M. Crystal structures of the red, yellow, and orange forms of mercuric iodide. *Inorg. Chem.* **1967**, *6*, 396.
(31) Pakhomov, V. I.; Goryunov, A. V.; Ivanova-Korfini, I. N.; Boguslavskii, A. A.; Lotfullin, R. S. Refinement of the Structure of $HgBr_2$. *Russ. J. Inorg. Chem.* **1990**, *35*, 1407.
(32) Braekken, H. T. The Crystal Structure of Lead Chloride, $PbCl_2$. *Z. Kristallogr.* **1932**, *83*, 222.
(33) Sass, R. L.; Brackett, E. B.; Brackett, T. E. The crystal structure of lead chloride. *J. Phys. Chem.* **1963**, *67*, 2863.
(34) Wang, X.; Andrews, L. Mercury dihydride forms a covalent molecular solid. *Phys. Chem. Chem. Phys.* **2005**, *7*, 750.
(35) Ebert, F.; Woitinek, H. Crystalline Structure of Fluorides. II. HgF, HgF_2, CuF and CuF_2. *Z. Anorg. Allg. Chem.* **1933**, *210*, 269.
(36) Özen, A. S.; Akdeniz, Z.; Pastore, G.; Ruberto, R.; Tosi, M. P. Structure of trimers of group-2B metal dihalides from relativistic density-functional calculations. *Phys. Chem. Liq.* **2015**, *53*, 1.
(37) Donald, K. J.; Stewart, J.; Guarino, M. Structure, bonding, relativistic effects, and dispersion in the group 12 dihalide $(MX_2)_3$ clusters, with lessons from the extended solids. *Struct. Chem.* **2015**, *26*, 1179.
(38) Schyck, S.; Evlyukhin, E.; Kim, E.; Pravica, M. High pressure behavior of mercury difluoride (HgF_2). *Chem. Phys. Lett.* **2019**, *724*, 35.
(39) Wang, X.; Li, J. The new phase of HgF_2 at high pressure. *Europhys. Lett.* **2013**, *102*, 36002.
(40) Giannozzi, P.; Baroni, S.; Bonini, N.; Calandra, M.; Car, R.; Cavazzoni, C.; Ceresoli, D.; Chiarotti, G.; Cococcioni, M.; Dabo, I.; et al. QUANTUM ESPRESSO: a modular and open-source software

https://doi.org/10.1021/acs.jpca.0c10847
J. Phys. Chem. A 2021, 125, 3978−3985

project for quantum simulations of materials. *J. Phys.: Condens. Matter* **2009**, *21*, 395502.
(41) Head-Gordon, M.; Head-Gordon, T. Analytic MP2 frequencies without fifth-order storage. Theory and application to bifurcated hydrogen bonds in the water hexamer. *Chem. Phys. Lett.* **1994**, *220*, 122.
(42) Perdew, J. P.; Burke, K.; Ernzerhof, M. Generalized Gradient Approximation Made Simple. *Phys. Rev. Lett.* **1996**, *77*, 3865.
(43) Grimme, S.; Antony, J.; Ehrlich, S.; Krieg, H. A consistent and accurate *ab initio* parametrization of density functional dispersion correction (DFT-D) for the 94 elements H-Pu. *J. Chem. Phys.* **2010**, *132*, 154104.
(44) Krogel, J. Nexus: A modular workflow management system for quantum simulation codes. *Comput. Phys. Commun.* **2016**, *198*, 154.
(45) Tran, F.; Kalantari, L.; Traoré, B.; Rocquefelte, X.; Blaha, P. Nonlocal van der Waals functionals for solids: Choosing an appropriate one. *Physical Review Materials* **2019**, *3*, No. 063602.
(46) Cooper, V. R.; Donald, K. J. First principles predictions of van der Waals bonded inorganic crystal structures: Test case. *Phys. Procedia* **2015**, *68*, 25.
(47) Hull, S.; Keen, D. A. Effect of hydrostatic pressure on the crystal structure and superionic behavior of lead (II) fluoride. *Phys. Rev. B: Condens. Matter Mater. Phys.* **1998**, *58*, 14837.
(48) Momma, K.; Izumi, F. VESTA 3 for three-dimensional visualization of crystal, volumetric and morphology data. *J. Appl. Crystallogr.* **2011**, *44*, 1272.

NOTE ADDED AFTER ASAP PUBLICATION

This paper was initially published March 16, 2021, with an incorrect copyright line. The copyright was corrected and the paper reposted April 30, 2021.

https://doi.org/10.1021/acs.jpca.0c10847
J. Phys. Chem. A 2021, 125, 3978−3985